

Article

Low Noise Interface ASIC of Micro Gyroscope with Ball-disc Rotor

Mingyuan Ren ¹ , Honghai Xu ¹, Xiaowei Han ^{2,*}, Changchun Dong ¹ and Xuebin Lu ¹

¹ School of Software and Microelectronics, Harbin University of Science and Technology, Harbin 150080, China; rmy2000@126.com (M.R.); honghai9960605@163.com (H.X.); hitdongcc@163.com (C.D.); lxbsw@126.com (X.L.)

² School of Computer and Information Engineering, Harbin University of Commerce, Harbin 150028, China

* Correspondence: hanxiaowei2017@163.com; Tel.: +86-451-8489-2063

Received: 21 January 2020; Accepted: 21 February 2020; Published: 24 February 2020



Abstract: A low noise interface ASIC for micro gyroscope with ball-disc rotor is realized in 0.5μm CMOS technology. The interface circuit utilizes a transimpedance pre-amplifier which reduces input noise. The proposed interface achieves 0.003°/s/Hz^{1/2} noise density and 0.003°/s sensitivity with ±100°/s measure range. The functionality of the full circuit, including circuit analysis, noise analysis and measurement results, has been demonstrated.

Keywords: low noise interface; micro gyroscope; capacitive detection

1. Introduction

Micro gyroscopes are small, inexpensive sensors that can measure angular rate or angle, which have increasingly taken the place of conventional rate sensors in many applications such as defense and consumer electronics [1]. Vibratory gyroscopes are the most common of the existing micro gyroscopes [2]. But it is difficult to reach tactical-grade and inertial-grade performance with these kinds of gyroscopes because of the structural constraint. Rotor gyroscope potentially has a higher performance than vibratory gyroscopes [3–5].

Noise isn't only an area of science and technology that poses practical problems but also has deep intellectual attractions [1]. The noise in micro gyroscopes includes both external noise and internal noise. The magnitude of external noise signals coupled into a gyroscope varies with the actual conditions. Mechanical thermal noise and circuit noise are the most important sources of internal noise in micro gyroscopes. Effectively reducing internal noise and improving the signal-to-noise ratio of the system are important challenge for gyroscope designers.

The mechanical noise exists widely in micro gyroscope structures, namely Brownian motion, and is caused by random impacts of molecules on a structure, it is commonly considered as the mechanical sensitivity limitation [6–9]. And the circuit noise includes electrical-thermal noise (Johnson noise), shot noise, flicker noise (1/f noise), demodulation phase noise, and so on. To reduce this noise, low-noise readout circuits have been reported [10–16]. But, the published papers mostly focus on vibratory micro gyroscope, and the noise analysis of rotor-type micro gyroscope is rarely mentioned. As the noise level affects the detection accuracy of micro gyroscope, it is urgent to carry out the research on the related theory and model of rotor micro gyroscope noise.

In order to improve the performance and detection accuracy of the rotor micro gyroscope, it is necessary to reduce the noise level of the system. At the same time, noise suppression is the core content of ASIC research on micro gyroscope interface. In this paper, the noise model of ASIC system with ball-disc rotor micro gyroscope interface will be established according to the unique damping characteristics and driving mode of ball-disc rotor micro gyroscope.

2. System Noise of Micro Gyroscope

The mechanical structure of the ball-disc rotor micro gyroscope is shown in Figure 1. According to the different sources of noise, system noise of the micro gyroscope can be divided into mechanical noise, driving noise and electronic noise.



Figure 1. Mechanical structure of micro gyroscope with ball-disc rotor.

2.1. Mechanical Noise

Considering mechanical noise is produced by the thermal motion of micro gyroscope rotor, the thermal motion equation of the micro gyroscope can be described as:

$$I\ddot{\alpha} + D\dot{\alpha} + E\alpha = F, \quad (1)$$

where F denotes the torque of the random thermal motion; I denotes the rotor moment of inertia; D denotes damping coefficient; E denotes the elastic coefficient, radial component coefficient of electromagnetic force.

When the system reaches thermal equilibrium, the spectral density of random wave moment of Brownian thermal motion is [11]:

$$F = \sqrt{4k_B TDB}, \quad (2)$$

where k_B is the Boltzmann constant, T is the absolute temperature, B is the noise bandwidth. The signal transfer function of the ball-disc rotor micro-gyro mechanical structure is given by:

$$S_{mech} = \frac{2I\omega R_2}{E} \Omega, \quad (3)$$

where ω is the rotor rotation speed, Ω is the input angular velocity, R_2 is the rotor ring radius. Then the signal-to-noise ratio of the micro gyroscope mechanical structure can be calculated by Equations (2) and (3).

$$SNR_{mech} = \frac{I\omega R_2 \Omega}{E \sqrt{k_B TDB}}, \quad (4)$$

According to this Equation (4), if the input angular velocity is given, the signal-to-noise ratio of the micro-gyro mechanical structure is proportional to the moment of inertia, rotor speed and rotor radius, and inversely proportional to the radial component coefficient of the electromagnetic force.

In order to express the relationship between the micro gyroscope structure and its corresponding noise characteristics, when the value of the input angular velocity is 1, the equivalent input angular velocity noise of the mechanical structure can be obtained:

$$\Omega_{mech} = \frac{E \sqrt{k_B TDB}}{I\omega R_2}, \quad (5)$$

where Ω_{mech} is the equivalent input angular velocity noise of mechanical structure. It can be known from Equation (5) that the equivalent input angular velocity noise of the mechanical structure is related

to the damping parameters, the moment of inertia, the elastic coefficient and the rotor speed. In the practical design, the mechanical noise can be reduced by decreasing the damping and electromagnetic force of the ball disk rotor or increasing the moment of inertia and speed of the ball disk rotor.

2.2. Driving Noise

The driving interference in the circuit refers to the interference caused by the electromagnetic driving of the micro gyroscope to the detection part of the system. The drive method of the ball dish rotor is electromagnetic drive, and the relationship between the corresponding drive interference fundamental frequency and the micro gyroscope rotor speed is:

$$\omega_0 = 2\pi \frac{N}{60}, \quad (6)$$

where N is the rotor rotation speed. The equivalent equation for driving interference coupled to the sense input is:

$$V_{n-d} = A_0 \sin \omega_0 t + A_1 \sin \frac{\omega_0}{2} t + \dots + A_n \sin \frac{\omega_0}{n+1} t + \dots, \quad (7)$$

where A_n is the amplitude of the n -th harmonic of the driving interference; ω_0 is the fundamental angular frequency of the drive disturbance. It can be known from Equation (7) that the driving interference noise is mainly affected by the rotor speed and the driving force. In order to effectively reduce the driving interference noise, a high-order low-pass filter needs to be used in the detection circuit.

When the angular velocity signal is input, the micro-gyro detection capacitance will change accordingly. The relationship between the two can be expressed as:

$$\Delta C = \frac{IR_2\omega}{E} \Omega C_0, \quad (8)$$

where C_0 is the nominal value of the detection capacitor. Then the signal-to-noise ratio of the driving interference can be calculated by Equations (7) and (8):

$$SNR_{driv} = \frac{IR_2\omega}{E} \Omega \frac{C_0}{A_0 \sin \omega_0 t}, \quad (9)$$

It can be known from Equation (9) that the signal-to-noise ratio of driving interference is proportional to the moment of inertia, rotor speed, rotor radius, and detection capacitance. Additionally, it is inversely proportional to the radial component coefficient of the electromagnetic force and the amplitude of the driving interference signal.

In order to express the relationship between the driving interference of the micro gyroscope and its corresponding noise characteristics, when the value of the input angular velocity is 1, the equivalent input angular velocity noise of the driving interference can be obtained:

$$\Omega_{driv} = \frac{EA_0 \sin \omega_0 t}{IR_2\omega C_0}, \quad (10)$$

where Ω_{driv} is the driving interference equivalent input angular velocity noise. It can be known from Equation (10) that the equivalent input angular velocity noise of the drive disturbance is related to the amplitude of the drive disturbance, the damping parameter, the moment of inertia, the detection capacitance, the elastic coefficient and the rotor speed. In actual design, driving noise can be reduced by using a high-order low-pass filter in the detection circuit.

The drive interference test chart of a ball-disc rotor micro-gyro through the back electromotive force detection is shown in Figure 2. The drive interference frequency is about 0.3 KHz. At this time, the rotor speed is 18,000 rpm, and the oscilloscope sampling period is 50 KHz. Using MATLAB to process the data in Figure 2, spectral characteristics of the micro-gyro driving noise can be obtained. As shown in Figure 3, the fundamental frequency of the driving noise is 0.293 KHz, which basically

matches the corresponding frequency of the rotor speed of 0.3 KHz. However, because the influence of driving noise on the output signal can be up to several hundred millivolts, the interference of driving noise must be eliminated. The effective bandwidth of the output signal is only one order of magnitude different from the driving noise. It is necessary to use higher order low-pass filter with more than six orders.

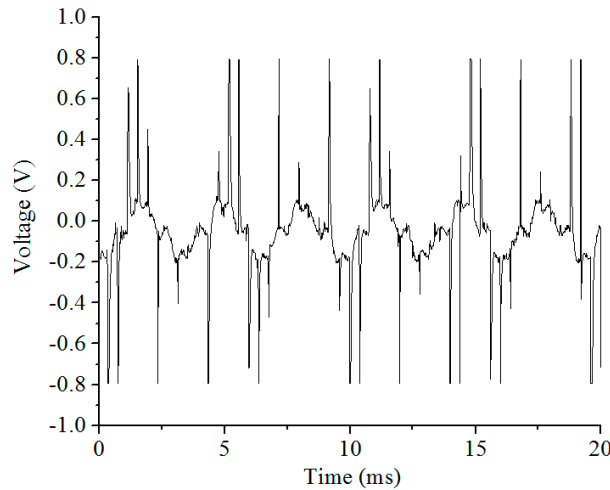


Figure 2. Test of driving interference for micro gyroscope with ball-disc rotor.

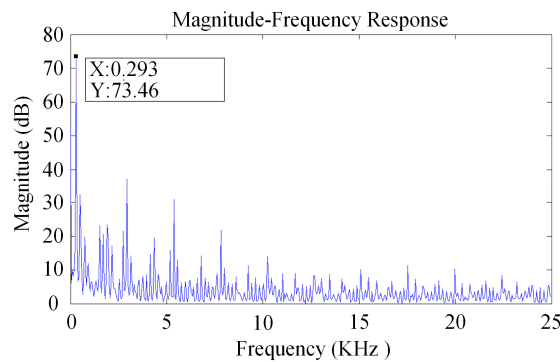


Figure 3. Frequency response of driving interference for micro gyroscope.

2.3. Electronic Noise

As shown in Figure 4, an open-loop system of multistage noise injection is proposed. According to Friis formula, the total equivalent input noise coefficient can be expressed as:

$$V_{in-noise} = V_{n1} + \frac{V_{n2} - 1}{A_1} + \frac{V_{n3} - 1}{A_1 A_2}, \tag{11}$$

where $V_{in-noise}$ is the total equivalent input noise coefficient; V_{ni} is the noise injection of level i ; A_N is the gain of n th stage.

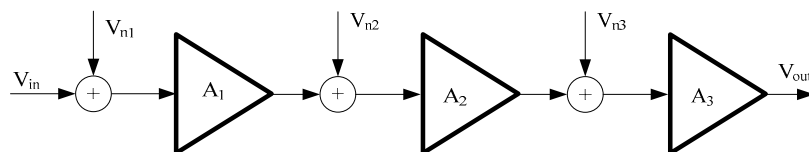


Figure 4. Noise of opened-loop system.

According to the relation of Equation (11), if the gain of the front stage amplifier is large enough, the sum of noise sources introduced by the rear stage can be ignored. The detection circuit of the micro gyroscope consists of the front stage transimpedance amplifier, the backstage amplifier, the modem and the low-pass filter. The main noise source of the micro gyro detection circuit can be considered to be from the front stage transimpedance amplifier, because the former stage transimpedance amplifier conforms to the previous assumption [17].

Figure 5 shows the noise model of the previous transimpedance amplifier. As shown in Figure 5, V_{rt} denotes the high-frequency excitation noise; C_s denotes the micro gyroscope sensitive structural capacitor; V_{n-am} denotes the input reference thermal noise of a transimpedance operational amplifier; R_{in} denotes the input impedance of a transimpedance operational amplifier; C_f denotes the feedback capacitor; R_f denotes the feedback resistor; V_{r1} denotes the feedback resistance thermal noise, A_0 denotes the dc gain of the transimpedance op amp [18,19].

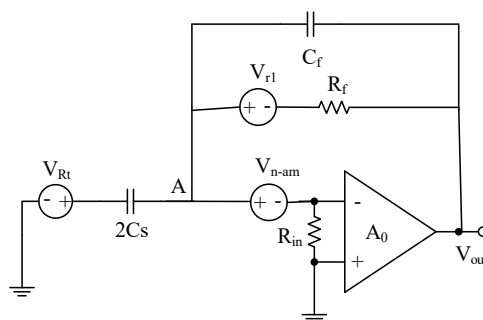


Figure 5. Noise model of the transimpedance amplifier.

According to Kirchhoff's circuit law and the characteristics of the amplifier, the equivalent input noise expression of the transimpedance amplifier can be obtained.

$$\begin{aligned} \frac{\overline{V_{n-in}^2}(f)}{\Delta f} &= \frac{V_{n-in}(f)V_{n-in}^*(f)}{\Delta f} = \left[\frac{(2C_s + C_f)^2}{2C_s} + \frac{1 + (2\pi f C_f R_f)^2}{(4\pi f C_s R_f)^2} \right] \\ &+ (2C_s + C_f) \frac{1 + 8\pi^2 f^2 C_s C_f R_f^2}{C_s (4\pi f C_s R_f)^2} \times \frac{\overline{V_{n-am}^2}(f)}{\Delta f} + \frac{\overline{V_{Rt}^2}(f)}{\Delta f} + \frac{kT}{4R_f (\pi f C_s)^2} \end{aligned} \quad (12)$$

Since $(2\pi f C_f R_f)^2 \gg 1$, $8\pi^2 f^2 C_s C_f R_f^2 \gg 1$, and R_f is very large, so Equation (12) can be further simplified as:

$$\frac{\overline{V_{n-in}^2}(f)}{\Delta f} = \left(\frac{C_s + C_f}{C_s} \right)^2 \frac{\overline{V_{n-am}^2}(f)}{\Delta f} + \frac{\overline{V_{Rt}^2}(f)}{\Delta f}, \quad (13)$$

If $C_f = 2C_s$, the Equation (13) can be simplified to:

$$\frac{\overline{V_{n-in}^2}(f)}{\Delta f} = \frac{9\overline{V_{n-am}^2}(f)}{\Delta f} + \frac{\overline{V_{Rt}^2}(f)}{\Delta f}, \quad (14)$$

From Equations (13) and (14), it can be known that the circuit noise is mainly determined by the front-stage transimpedance amplifier noise, high-frequency excitation noise, and C_f/C_s . The noise of the circuit can be effectively reduced by decreasing the above correlation items, but it will increase the difficulty of circuit design.

The signal-to-noise ratio of the micro gyroscope detection circuit can be calculated by Equations (8) and (14):

$$SNR_{cir} = \frac{I\omega R_2 \Omega}{E} \frac{C_0}{\left(\frac{C_s + C_f}{C_s} \right)^2 \frac{\overline{V_{n-am}^2}}{\Delta f} + \frac{\overline{V_{Rt}^2}}{\Delta f}}, \quad (15)$$

According to Equation (15), when the input angular velocity is constant, the signal-to-noise ratio of the micro-gyro detection circuit is proportional to the moment of inertia, rotor speed, rotor radius, and detection capacitance; it is inversely proportional to the radial component coefficient of the electromagnetic force.

In order to express the relationship between the micro gyroscope detection circuit and its corresponding noise characteristics, when the value of the input angular velocity is 1, the equivalent input angular velocity noise of the detection circuit is defined as:

$$\Omega_{cir} = \frac{E[(\frac{C_s+C_f}{C_s})^2 V_{n-am}^2 + V_{Rt}^2]}{I\omega R_2 C_0}, \quad (16)$$

where Ω_{cir} is the detection circuit equivalent input angular velocity noise. It can be known from Equation (16) that the equivalent input angular velocity noise of the detection circuit is related to the previous stage transimpedance amplifier noise, high-frequency excitation noise, C_f/C_s , damping parameters, moment of inertia, detection capacitance, elastic coefficient, and rotor speed. In the actual design, the noise of the detection circuit can be reduced by optimizing the noise of the pre-stage transimpedance amplifier, high-frequency excitation noise, and C_f/C_s .

According to the different sources of noise, the noise of micro-gyroscope system can be divided into driving interference noise, mechanical noise and electronic noise. In the process of modeling, the mechanical noise caused by the thermal movement of molecules on the surface of sensitive structures, the driving interference caused by the electromagnetic driving of micro-gyroscopes and the circuit noise in the interface circuit are analyzed theoretically. As shown in Table 1, the correctness of the model is verified by the calculated values of the equivalent input angular velocity of system noise.

Table 1. Calculated values of equivalent input angular velocity noise of gyroscope system.

Micro Gyroscope Noise Source	Equivalent Input Angular Velocity	Calculated Value ($^{\circ}/s/Hz^{1/2}$)
Structural Thermal Sensitive Noise	$\Omega_{mech} = \frac{E\sqrt{k_B TDB}}{IR_2\omega}$	6.1×10^{-4}
Driving Interference Noise	$\Omega_{driv} = \frac{EA_0 \sin \omega_0 t}{IR_2\omega C_0}$	4.6×10^{-3}
Detecting Circuit Noise	$\Omega_{cir} = \frac{E[(\frac{C_s+C_f}{C_s})^2 V_{n-am}^2 + V_{Rt}^2]}{IR_2\omega C_0}$	1.8×10^{-5}

The equivalent input noise of the preamplifier can be calculated by dividing the output noise of the micro gyroscope system by the loop gain. The SNR of the low noise amplifier is:

$$SNR = \frac{V_{sig}}{V_{on}} = \frac{V_s(\frac{\Delta C}{C_F})}{\sqrt{2}V_{n-in}(1 + \frac{C_S}{C_F})}, \quad (17)$$

where V_{sig} is the output of the preamplifier; V_{on} is the output noise of the pre amplifier; V_s is the input signal of the pre amplifier; V_{n-in} is the equivalent input noise of the preamplifier.

According to Equation (17), the change rate of relative capacitance can be obtained as shown in Equation (18):

$$\frac{\Delta C}{C_S} = \frac{\sqrt{2}V_{n-in}(1 + \frac{C_F}{C_S})}{V_s} = \frac{2V_{n-in}(1 + \frac{C_F}{C_S})}{V_{DD} - V_{SS}}, \quad (18)$$

From Equation (18), the minimum resolution of the system is proportional to the input noise. With the decreasing of input noise, the detection resolution of the system can be improved accordingly.

3. Low Noise Interface Circuits

In Figure 6, four pairs of differential detection capacitors (C_1, C_2, C_3 and C_4 are variable capacitors between the upper plate and the rotor; C_5, C_6, C_7 and C_8 are variable capacitors between the lower plate and the rotor) are used to represent the simplified equivalent model of the structure of the micro gyroscope. The driving circuit consists of OP1 and OP2 and their corresponding peripheral components, which generates sinusoidal excitation signals with equal amplitude and opposite phase. The excitation signals are loaded on the upper and lower electrodes of the gyroscope structure respectively. When the gyro rotor deflects in the X+ direction, C_1 and C_5 also change accordingly. The differential capacitance changes through charge-voltage conversion circuit composed of OP3, AC amplifier circuit composed of OP4, phase-sensitive demodulation circuit and LPF1 low-pass filter. The displacement output signal V_{out11} in the X+ direction is obtained. At the same time, the displacement output signal V_{out1} is amplified by the afterburner circuit K_1 and K_5 to form a feedback voltage-loaded differential capacitor on the control electrodes of C_1 and C_5 , so that the rotor can return to the balanced position in the X+ direction. Similarly, changes in other directions can be obtained.

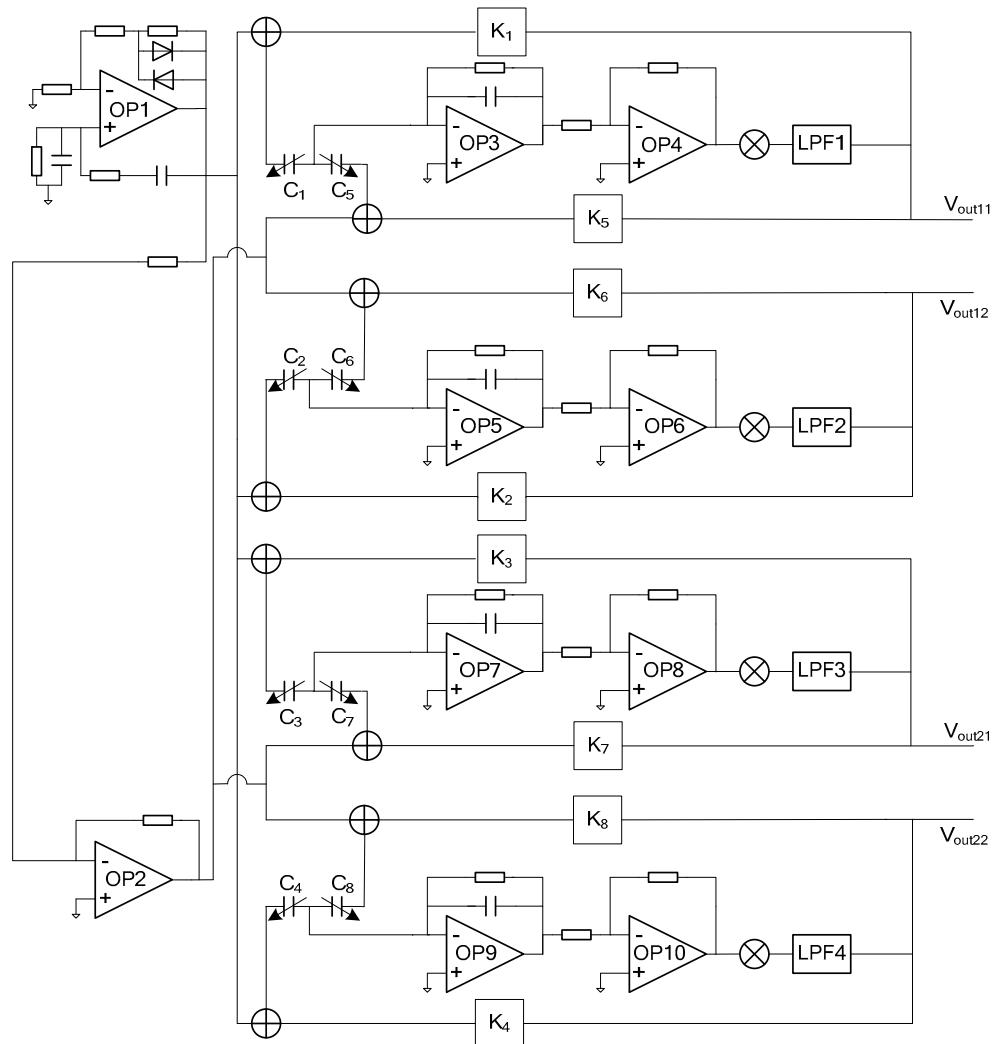


Figure 6. Overall realization scheme for the interface ASIC of micro gyroscope with ball-disc rotor.

As shown in Figure 7, there is a single path rotor displacement detection circuit in x -axis direction, including preamplifier, AC amplifier, phase sensitive demodulation unit, low-pass filter and other modules.

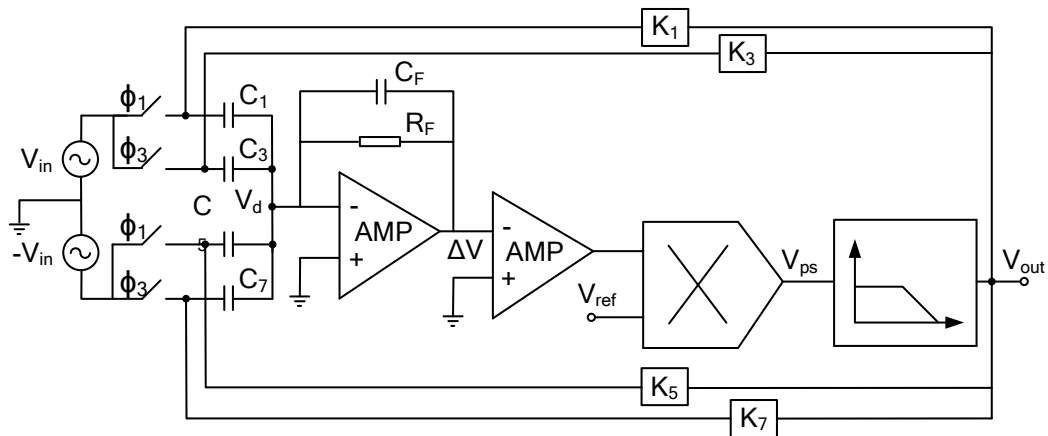


Figure 7. Schematic of the single path detection principle of micro gyroscope with ball-disc rotor.

The charge-voltage conversion circuit structure of the transimpedance structure is shown in Figure 8. In order to improve the open-loop gain, a three-stage folded cascode structure is used in the operational amplifier. Through the analysis of its structure, the equivalent input noise density is obtained as follows:

$$V_n^2 = \frac{16kT}{3} \left(\frac{1}{g_{m2}} + \frac{g_{m5} + g_{m8}}{g_{m2}^2} \right) \quad (19)$$

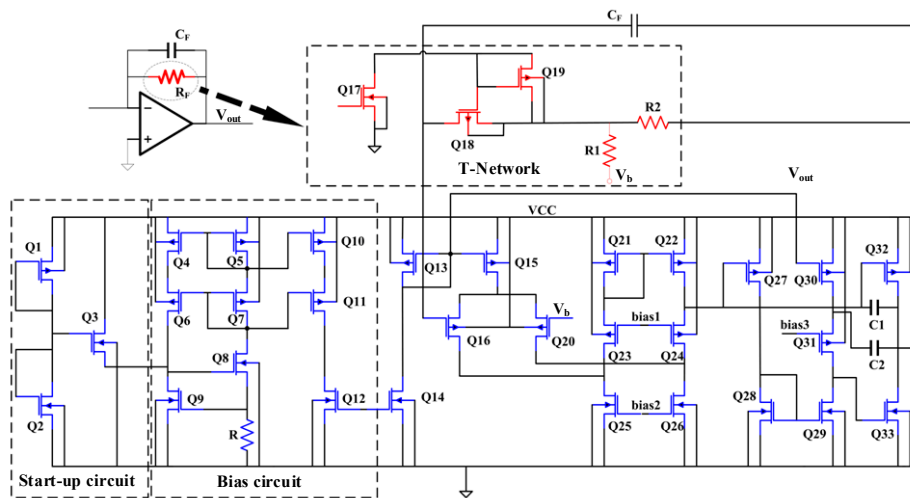


Figure 8. Transimpedance structure of charge voltage conversion circuit.

T-type topology is adopted to achieve the high resistance required by the trans-resistance structure. Among them, Q17 and Q19 are set to make Q18 obtain smaller gate voltage, and the transistor Q18 is designed as a long channel type, that is, smaller W/L. At this time, Q18 works in linear region, its resistance can reach Mega level, and its working characteristics can be guaranteed by the corresponding bias circuit. The equivalent resistance of T-type network is obtained as follows:

$$R_{eq} = R_M \left(1 + \frac{R_2}{R_1} \right) + R_2 \quad (20)$$

R_M is the resistance value of transistor Q18 in linear region. When the resistance of transistor Q18 is much larger than that of resistors R_1 and R_2 in Figure 8, Equation (20) shows that if the resistance of transistor Q18 is greater than 1 M Ω , the main noise source of charge-voltage conversion circuit is the

equivalent resistance of transistor Q18. In this case, the output signal-to-noise ratio can be expressed as follows.

$$SNR = \sqrt{\frac{I_{IN}^2 R_{eq}}{4KT(R_2/R_1 + 1)}} \approx \sqrt{\frac{I_{IN}^2 R_M}{4KT}}, \quad (21)$$

where I_{IN} is input signal of the charge-voltage conversion circuit. The regular expression is defined as follows.

$$I_{IN} = \frac{\partial C}{\partial t} V_b = C_0 V_b \omega \sin \omega t, \quad (22)$$

where C_0 is maximum change value of the sensitive capacitance of the exciting electrode; V_b is forward bias voltage charge voltage conversion circuit; ω is driving mode resonance frequency. The combination Equations (21) and (22) show that the signal-to-noise ratio is mainly determined by the resistance of transistor Q18 and the bias voltage V_b .

4. Results and Discussion

The performance of the interface ASIC designed in this paper and the interface ASIC performance in the main literature are shown in Table 2. The relative capacitance change rates shown in the table are calculated from the measured values according to Equation (26). The vibrating micro-gyro interface ASIC designed by the University of California, Berkeley has achieved a relative capacitance change rate of 1.3×10^{-8} , and its Sigma-Delta force feedback structure and related double sampling technology have reduced circuit noise requirements [20]. The continuous time current (CTC) sensitive circuit designed by the Technical University of Helsinki, Finland can avoid the noise coupling phenomenon of the switched capacitor circuit; the relative capacitance resolution reaches 9×10^{-8} [21]. The quadrature frequency-modulated micro-gyro designed by the University of California, Berkeley uses Frequency Modulation (FM) technology, and the relative capacitance resolution reaches 1.67×10^{-8} [22]. The Indian University of Science and Technology reported the use of bulk silicon process accelerometer switched capacitor detection circuit, whose relative capacitance resolution can reach 4.94×10^{-9} [23].

Table 2. Comparison of reported works of interface ASIC with this work.

	Sensor Type	Circuit Structure	Static Capacitance (pF)	Sensitivity	Noise Density	Resolution ($\Delta C_{MIN}/CS$)
[19]	gyroscope	SC	—	—	$0.004^\circ/s/Hz^{1/2}$	1.3×10^{-8}
[20]	accelerometer	CTC	12	3.8 pF/g	$0.3 \mu g/Hz^{1/2}$	9×10^{-8}
[21]	gyroscope	FM	6×10^{-3}	—	$0.09^\circ/s/Hz^{1/2}$	1.67×10^{-8}
[22]	accelerometer	SC	0.88	4.576 fF/g	—	4.94×10^{-9}
This paper	gyroscope	CTC	5	$0.003^\circ/s$	$0.003^\circ/s/Hz^{1/2}$	1×10^{-8}

The layout is based on a high voltage $0.5 \mu m$ 2P2M N well CMOS process. The layout of the spherical disc rotor micro-gyroscope is shown in Figure 9. The layout area is 19.49 mm^2 . Figure 10 is the output signal noise spectrum of dynamic signal analyzer HP35670A. The test results show that the noise spectral density of interface ASIC at 10 Hz is $44.7 \text{ mV}/Hz^{1/2}$, which is equivalent to the input noise of the system, $0.003^\circ/s/Hz^{1/2}$. Test results of the interface circuit for micro gyroscope with ball-disc rotor are shown in Table 3.

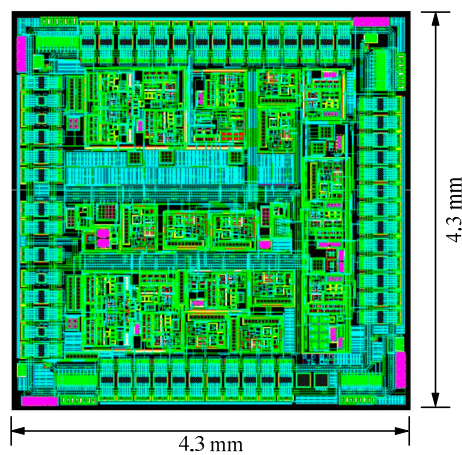


Figure 9. Layout of the interface circuit for micro gyroscope with ball-disc rotor.

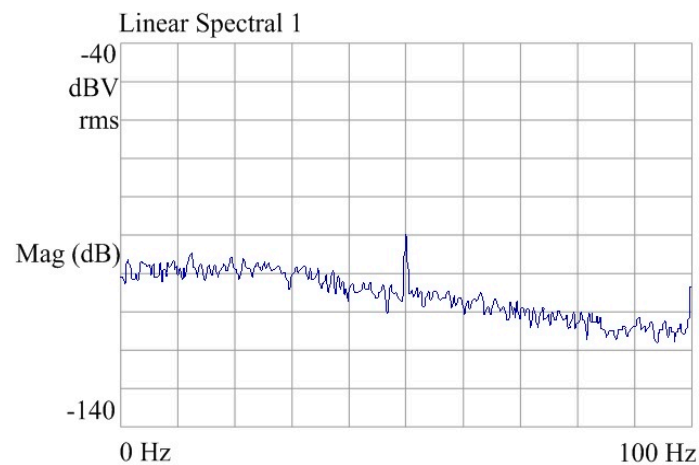


Figure 10. Spectrum of system output noise.

Table 3. Test results of the interface circuit for micro gyroscope with ball-disc rotor.

Parameters	Measurements
Supply voltage (V)	± 9
Area (mm^2)	4.9×4.9
Power dissipation (mW)	30
Flicker noise corner (kHz)	100
Output voltage range (V)	-8.6 – $+8.3$
Non-linear (%)	0.02
System output noise at 10 Hz ($\text{mV}/\text{Hz}^{1/2}$)	44.7

As can be seen from Table 4, compared with the performance parameters of the rotor gyroscope published in recent years, the ball-disc rotor micro-gyroscope designed in this paper has low noise and high linearity, and can obtain more accurate angular velocity measurements in some occasions with high accuracy requirements.

Table 4. Comparison of reported works with this work.

Parameters	[24]	[25]	This Paper
Maximum Rotor Speed (rpm)	58,000	12,000	20,000
Nonlinear Error (%)	0.1%	0.58%	0.05%
Noise Density ($^{\circ}/s/Hz^{1/2}$)	0.03	0.015	0.003
Measure Range (o/s)	± 200	± 100	± 100
Bandwidth (Hz)	10	10	10
Sensitivity ($^{\circ}/s$)	0.1	0.014	0.003
Scale Factor (mV/ $^{\circ}/s$)	-	39.8	15

5. Conclusions

In this work, we describe a low noise interface ASIC for micro gyroscope with ball-disc rotor. The transimpedance pre-amplifier of the proposed circuit effectively addresses thermal and flicker noise issues. The measurement results for the circuit implemented in a 0.5 μm CMOS technology show an equivalent to the input noise of the system, 0.003 $^{\circ}/s/Hz^{1/2}$ and a sensitivity of 0.003 $^{\circ}/s$ with $\pm 100^{\circ}/s$ measure range.

Author Contributions: Conceptualization, M.R.; Methodology, M.R. and C.D.; validation, M.R. and H.X.; Writing—Original Draft Preparation, M.R. and H.X.; Writing—Review and Editing, M.R., H.X. and X.H.; Supervision, C.D. and X.L.; Funding Acquisition, X.H. All authors regularly discussed the progress during the entire work. All authors have read and agreed to the published version of the manuscript.

Funding: This work was supported by the Fundamental Research Foundation for Universities of Heilongjiang Province (Grant No. LGYC2018JC018) and supported by the Heilongjiang Province Natural Science Foundation (Grant No. F2018020, F2018018).

Conflicts of Interest: The authors declare no conflict of interest.

References

1. Mohd-Yasin, F.; Nagel, D.J.; Korman, C.E. Noise in MEMS. *Meas. Sci. Technol.* **2009**, *21*, 012001. [[CrossRef](#)]
2. Piyabongkarn, D.; Rajamani, R.; Greminger, M. The development of a MEMS gyroscope for absolute angle measurement. *IEEE Trans. Control Syst. Technol.* **2005**, *13*, 185–195. [[CrossRef](#)]
3. Liu, K.; Zhang, W.; Chen, W.; Li, K.; Dai, F.; Cui, F.; Wu, X.; Ma, G.; Xiao, Q. The development of micro-gyroscope technology. *J. Micromech. Microeng.* **2009**, *19*, 113001. [[CrossRef](#)]
4. Ren, M.Y.; Zhang, H.F.; Liu, X.W.; Mao, Z.G. High resolution capacitance detection circuit for rotor micro-gyroscope. *AIP Adv.* **2014**, *4*, 031336. [[CrossRef](#)]
5. Li, H.; Liu, X.W.; Weng, R.; Zhang, H.F. Micro-angle tilt detection for the rotor of a novel rotational gyroscope with a 0.47 "resolution. *Front. Inf. Technol. Electron. Eng.* **2017**, *18*, 591–598. [[CrossRef](#)]
6. Gabrielson, B. Mechanical–thermal noise in acoustic and vibration sensors. *IEEE Trans. Electron. Devices* **1993**, *40*, 903–909. [[CrossRef](#)]
7. Annovazzi-Lod, V.; Merlo, S. Mechanical–thermal noise in micromachined gyros. *Microelectron. J.* **1999**, *30*, 1227–1230. [[CrossRef](#)]
8. Djurić, Z. Mechanisms of noise sources in microelectromechanical systems. *Microelectron. Reliab.* **2000**, *40*, 919–932. [[CrossRef](#)]
9. Leland, R.P. Mechanical-thermal noise in MEMS gyroscopes. *IEEE Sens. J.* **2005**, *5*, 493–500. [[CrossRef](#)]
10. Sun, H.; Jia, K.; Liu, X.; Yan, G.; Hsu, Y.W.; Fox, R.M.; Xie, H. A CMOS-MEMS gyroscope interface circuit design with high gain and low temperature dependence. *IEEE Sens. J.* **2011**, *11*, 2740–2748. [[CrossRef](#)]
11. Kim, D.; M'Closkey, R.T. Spectral analysis of vibratory gyro noise. *IEEE Sens. J.* **2013**, *13*, 4361–4374. [[CrossRef](#)]
12. Su, T.H.; Nitzan, S.H.; Taheri-Tehrani, P.; Kline, M.H.; Boser, B.E.; Horsley, D.A. Silicon MEMS disc resonator gyroscope with an integrated CMOS analog front-end. *IEEE Sens. J.* **2014**, *14*, 3426–3432. [[CrossRef](#)]
13. Xie, J.; Shen, Q.; Hao, Y.; Chang, H.; Yuan, W. Design, Fabrication and Characterization of a Low-noise Z-axis Micromachined Gyroscope. *Microsyst. Technol.* **2015**, *21*, 625–630. [[CrossRef](#)]

14. Shen, C.; Li, J.; Zhang, X.; Shi, Y.; Tang, J.; Cao, H.; Liu, J. A noise reduction method for dual-mass micro-electromechanical gyroscopes based on sample entropy empirical mode decomposition and time-frequency peak filtering. *Sensors* **2016**, *16*, 796. [[CrossRef](#)]
15. Ding, X.; Jia, J.; Gao, Y.; Li, H. Mechanical and electrical noise in sense channel of MEMS vibratory gyroscopes. *Sensors* **2017**, *17*, 2306. [[CrossRef](#)]
16. Utz, A.; Walk, C.; Haas, N.; Fedtschenko, T.; Stanitzki, A.; Mokhtari, M.; Görtz, M.; Kraft, M.; Kokozinski, R. An ultra-low noise capacitance to voltage converter for sensor applications in 0.35 μm CMOS. *J. Sens. Sens. Syst.* **2017**, *6*, 285. [[CrossRef](#)]
17. Wang, Y.T.; Yang, Z.; Cheng, P.F.; Li, H.J. Analysis of circuit noise in integral electronics piezoelectric accelerometer. *J. Appl. Sci. Eng.* **2015**, *18*, 295–302.
18. Sutri, N.Y.; Dennis, J.O.; Khir, M.H.M.; Mian, M.U.; Tang, T.B. Chopper stabilized, low-power, low-noise, front end interface circuit for capacitive CMOS MEMS sensor applications. *Mod. Appl. Sci.* **2013**, *7*, 34–42. [[CrossRef](#)]
19. Seraji, N.E.; Yavari, M. On the design and optimization of a switched-capacitor interface circuit for MEMS capacitive sensors. In Proceedings of the 2012 20th Iranian Conference on Electrical Engineering (ICEE), Tehran, Iran, 15–17 May 2012; pp. 286–290.
20. Ezekwe, C.D.; Boser, B.E. A mode-matching closed-loop vibratory gyroscope readout interface with a 0.004/s/noise floor over a 50 Hz band. *IEEE J. Solid-State Circuits* **2008**, *43*, 3039–3048.
21. Aaltonen, L.; Halonen, K. Continuous-time interface for a micromachined capacitive accelerometer with NEA of 4 g and bandwidth of 300 Hz. *Sens. Actuators A Phys.* **2009**, *154*, 46–56. [[CrossRef](#)]
22. Kline, M.H.; Yeh, Y.C.; Eminoglu, B.; Najjar, H.; Daneman, M.; Horsley, D.A.; Boser, B.E. Quadrature FM gyroscope. In Proceedings of the 2013 IEEE 26th International Conference on Micro Electro Mechanical Systems (MEMS), Taipei, Taiwan, 20–24 January 2013; pp. 604–608.
23. Krishnan, G.; Kshirsagar, C.U.; Ananthasuresh, G.K.; Bhat, N. Micromachined high-resolution accelerometers. *J. Indian Inst. Sci.* **2012**, *87*, 333–361.
24. Terasawa, T.; Watanabe, T.; Murakoshi, T. Electrostatically levitated ring-shaped rotational-gyro/accelerometer using all-digital OFDM detection with TAD. In Proceedings of the IEEE Sensors 2012, Taipei, Taiwan, 28–31 October 2012; pp. 1–4.
25. Han, F.T.; Liu, Y.F.; Wang, L.; Ma, G.Y. Micromachined electrostatically suspended gyroscope with a spinning ring-shaped rotor. *J. Micromech. Microeng.* **2012**, *22*, 105032. [[CrossRef](#)]



© 2020 by the authors. Licensee MDPI, Basel, Switzerland. This article is an open access article distributed under the terms and conditions of the Creative Commons Attribution (CC BY) license (<http://creativecommons.org/licenses/by/4.0/>).